

Comparison Between Photoactivity of ZnO/NiO Nanostructures Synthesized by CBD and Modified -CBD for Rhodamine B Removal

Sahar M. Ali*, Osama A. Dakhil, Emad H. Hussein

Department of Physics, College of Science, Mustansiriyah University, Baghdad, IRAQ.

*Correspondent contact: saharmohamed@uomustansiriyah.edu.iq

Article Info

Received
13/07/2021

Accepted
01/08/2021

Published
20/11/2021

ABSTRACT

This work describes a comparative study on zinc oxide/nickel oxide (ZnO/NiO) nanostructures deposited on glass substrates by chemical bath and modified bath, (CBD), and (M-CBD) techniques. The photoactivity of ZnO/NiO nanostructure films was tested on Rhodamine B (RB) dye under sunlight. The nanostructure films were evaluated using various characterization tools. Accordingly, the field-emission scanning electron microscopic (FE-SEM) images confirm that the film synthesized by CBD was flower-like nanosheet with a thickness of 37.96 - 51.36 nm. In contrast, the M-CBD film showed spherical nanoparticles with a diameter of 35.73 - 49.12 nm and nanosheet of a thickness of 42.43 nm. However, both films were then subject to sunlight for 150 min. The photocatalytic efficiencies of the CBD and M-CBD films were calculated to be 76 % and 92 %, respectively. It is thus concluded that enhancing the photocatalytic degradation for the removal of RB is demonstrated by modifying the classical CBD technique.

KEYWORDS: ZnO/NiO Nano-heterostructures; Photodegradation of Rhodamine B; Modified-Chemical Bath Deposition.

INTRODUCTION

Recently, wide-bandgap materials as photocatalysts for organic degradation in wastewater have been extensively [1]. The low-cost ZnO has been selected as a photocatalyst due to its strong oxidizing ability and eco-friendly substance [2, 3]. Also, NiO has been utilized in photocatalytic applications because of increasing the activity of the generation of electron-hole and enhancing the degradation mechanism [4, 5]. Ezhilarasi and Vijya reported the features of NiO nanoparticles (NPs) as a photocatalytic material [6]. Also, Duan et al. fabricate NiO NPs for

photodegradation of RB dye under ultraviolet energy [7]. To facilitate the transportation of charges and reduce the charge recombination, which increases photocatalytic efficiency, ZnO should be modified by doping, for example, with metal ions [8,9], noble-metal deposition [10], or coupling to oxides [11,12]. Therefore, it is usually that ZnO is coupled with different materials forming heterostructures such as ZnO/TiO₂, ZnO/SnO₂, and ZnO/ZnS [13]. In addition, as listed in Table 1, ZnO was fabricated for the photodegradation of RB using different techniques.

Table 1. The Materials used in different works, Organic pollutants, Techniques, Degradation time (min), and Degradation efficiency (%), and the Degradation efficiency (%) of Previous researches that used ZnO for removal RB.

Ref.	Materials	Organic pollutants	Techniques	Degradation time (min)	Degradation efficiency (%)
[14]	NiO/ZnO Hetero-junctions	Rhodamine B (10 mg/L)	facile electrospinning	50	86.6
[15]	ZCB (Zinc oxide impregnated chitosan beads)	Rhodamine B (50 mg/L)	chemical technique	60	68.4
[16]	ZnO/CoMoO ₄ nanocomposites	Rhodamine B (10 mg/L)	calcination process	300	90
[17]	ZnO and Cu ₂ O thin films	Rhodamine B (10 mg/L)	DC sputtering and pulsed laser deposition	360	61 and 43
[18]	Zinc oxide nanoparticles	Rhodamine B (10 mg/L)	Monochloro- acetic acid as a complexing agent	150	56.80

This research aims to enhance the photocatalytic activity of the ZnO/NiO nanostructures. Consequently, the effect of synthesis technique on such property was necessary to be studied. Furthermore, the degradation of RB would help the removal of this contaminant during water purification.

EXPERIMENTAL

Materials

All the chemical materials listed in Table 2 were used without any additional purification.

Table 2. The materials used in this work.

Material	Purity (%)	Company
Zinc nitrate hexahydrate Zn (NO ₃) ₂ .6H ₂ O	98.5	Scharlau, Spain
Nickel nitrate hexahydrate Ni (NO ₃) ₂ .6H ₂ O	99	AAG, Espana
Hexamethylenetetramine HMT, C ₆ H ₁₂ N ₄	99	Hi-media India
Absolute ethanol C ₂ H ₅ OH	100	Hayman, Uk
Rhodamine B Dye C ₂₈ H ₃₁ ClN ₂ O ₃	98.5	Sigma-Aldrich, Germany
Glass Substrate	-	Yingke Optical Products

Substrate Preparation

After ultrasonic cleaning of the glass substrates with ethanol and distilled water (DI), a seed layer of gold (Au) had been deposited on the substrates for one minute using a DC-Sputtering System (GSL-1100X-SPC 16-3, MTI Corporation) under a vacuum of 0.25 mbar. That was followed by environmentally thermal annealing of the layers at 500 °C for 2 hours.

Synthesis of ZnO/NiO Nanostructures

The Synthesis process started with the well-known CBD route was followed by another stage of ZnO/NiO nanostructures modification.

Synthesis by CBD

In this technique, 0.02 M of Zn (NO₃)₂.6H₂O, 0.01 M of (Ni (NO₃)₂.6H₂O), and 0.02M of HMT were mixed in 80 ml of DI with 10 min stirring keeping a pH value of 6. The seed layer was submerged inside the CBD cell at a temperature of 90 °C for 3 hours. After depositing the film, it was cleaned with DI and then dried at 60 °C for 10 minutes using a hotplate followed by thermal treatment at 400 °C for one hr.

Synthesis by M-CBD

In this technique, 0.02M (Zn (NO₃)₂.6H₂O) and 0.02 M of HMT were mixed and stirred in 80 ml of DI for 10 min. Then, after obtaining the ZnO film in a similar way to the previous technique, a second step started by adding a solution of 0.01 M (Ni (NO₃)₂.6H₂O) and 0.01 M of HMT to the resulting ZnO film. The synthesized film was thermally annealed at 400 °C for 1 hr.

Photocatalytic Degradation

The photoactivity of the nanostructures was evaluated for the degradation of RB aqueous solution with subjecting to sunlight. Under a wide range of wavelengths, the absorption peak of RB solution was determined at 550 nm. The prepared film was submerged in 50 mL of 10 mg/L RB solution for 30 min under darkness to perform absorption of the contaminants accumulated on the surface. Then, the absorption spectra were recorded in the darkness and after exposure to the sunlight for 150 min. The photocatalytic efficiency (*P*) can simply be estimated by

$$P = \frac{C_o - C_t}{C_o} \times 100 \% \quad (1)$$

considering *C*₀ (mg l⁻¹) and *C*_{*t*} (mg l⁻¹) are the concentrations of dye before and after light exposure.

RESULTS AND DISCUSSION

FE-SEM Images

The FE-SEM images ZnO/NiO Nanostructure prepared by CBD and M-CBD are shown in Figure 1. In the CBD film, nanosheets of flower-like shape with a thickness of 37.96 - 51.36 nm are seen in Figure 1-a. The cross-section thickness of the film is about 1.982 μm, as shown in Figure 1-b. In the M-CBD film, two structures were noticed: nanoparticles of spherical shape with diameters of 35.73 - 49.12 nm, and nanosheets of a thickness of 42.43 nm, as shown in Figure 1-c. The thickness of the film is seen in the cross-section image which is 1.072 μm, as shown in Figure 1-d.

XRD Curves

XRD of the CBD Film

Figure 2 shows the XRD curves of the ZnO/NiO nanostructure prepared by the CBD technique. The peaks, seen at 31.79° (100), 34.57° (002), 36.29° (101), 47.60° (102), 56.62°(110), and 68.0° (112), indicate the hexagonal phase of ZnO matching with the standard peaks (JCPDS 76-0704). The strong

peaks at (100) and (101) planes refer to the preferable orientation along with these directions [19]. The other peaks, seen at 38.24° (101), 42.93

(012), and 63.0° (104), are indexed in the cubic phase of NiO matching with the standard card (JCPDS 44-1159).

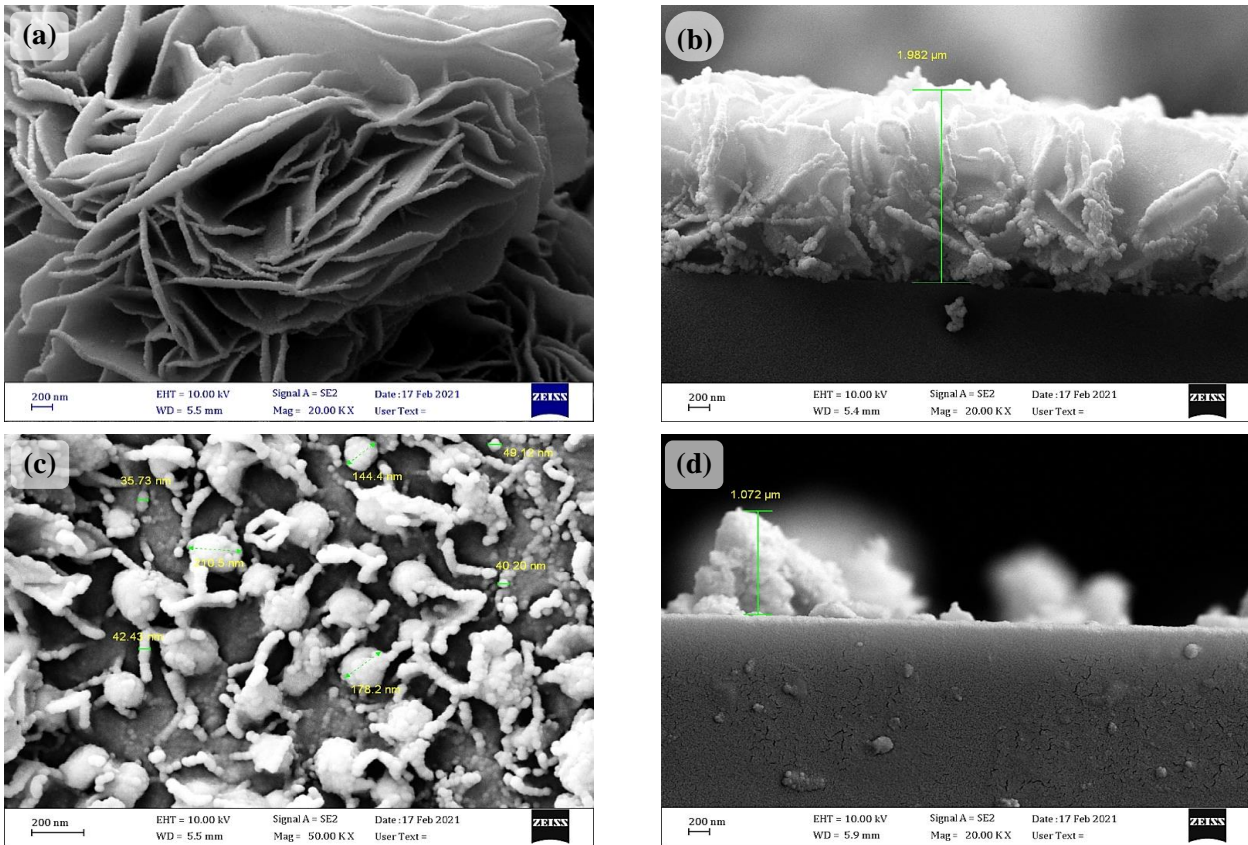


Figure 1. The FE-SEM images of the ZnO/NiO nanostructures were prepared by (a, b) CBD, and (c, d) M-CBD techniques. (All the scale bars are 200 nm)

XRD of the M-CBD Film

The XRD curves of the ZnO/NiO nanostructure prepared by M-CBD are shown in Figure 3. The peaks of 31.82° (100), 34.49° (002), 36.30° (101), 47.62° (102), 56.66°(110), 67.99° (112), and

69.34° (201) correspond to the hexagonal structure of ZnO (JCPDS 76-0704). Also, the cubic phase of NiO is confirmed at 38.25° (101), 43.0° (012), and 62.94° (104) (JCPDS 44-1159).

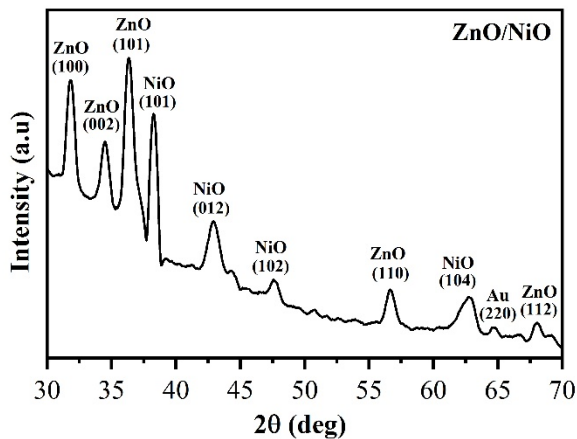


Figure 2. The XRD curve of the ZnO/NiO nanostructures fabricated by the CBD technique.

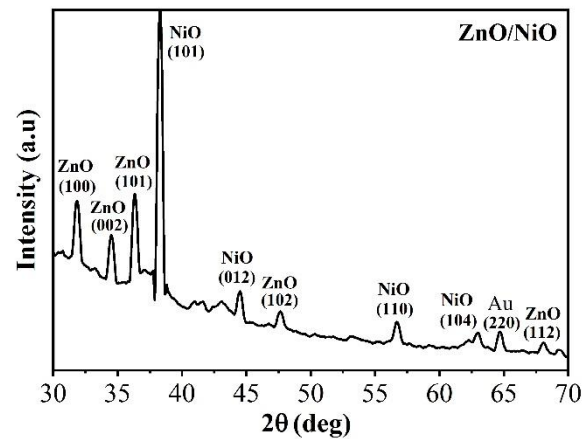


Figure 3. The XRD curve of the ZnO/NiO nanostructure fabricated by the M- CBD technique.

3.3. UV-Vis Spectroscopy

The absorption spectrum of the nanostructure films was recorded using a UV-vis spectrophotometer (Double Beam Li- 2800) and (T60, London). The absorption edge of the CBD film is determined at 349 nm whereas the M- CBD film shows the edge at 361 nm, as shown in Figure 4.

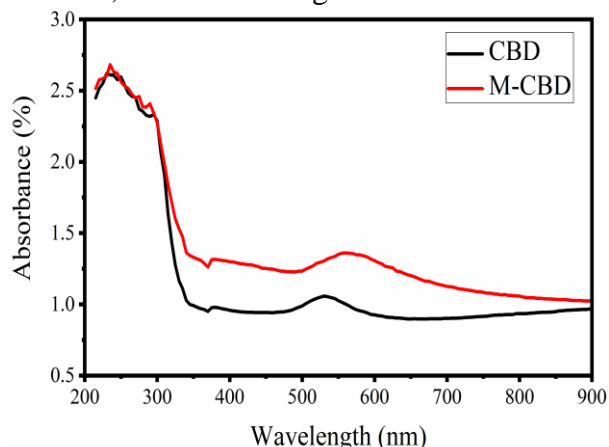


Figure 4. The UV-Vis absorption of the ZnO/NiO nanostructures prepared by the CBD, and the M-CBD techniques.

The direct energy bandgaps ($E_g(\text{dir})$) of both samples were calculated from $(\alpha h\nu)^2$ versus photon energy ($h\nu$) plot shown in Fig. 5. The $E_g(\text{dir})$ values of the CBD and M-CBD ZnO/NiO films were found to be 3.55 eV and 3.43 eV, respectively. These values are related to the direct energy gap of ZnO after the formation of heterojunction [20]. If the first value, for example, is compared with energy gaps of ZnO and NiO, one sees that value lies in between them. Therefore, when ZnO and NiO are coupled, the electrons transferred from NiO, whose Fermi level is higher, to ZnO of the lower level, a heterojunction is formed. Consequently, the energy gap of the heterostructure will change, resulting in a blue shift [21]. However, the small shift in the energy gap may be caused by the variation of the crystalline size throughout the sample or strain induced in ZnO causing quantum confinement in the heterostructures [22, 23]. Furthermore, the ZnO/NiO heterostructure has already experienced two types of bandgap transition. Hence, the indirect bandgap of the film prepared by the CBD route was extrapolated using $(\alpha h\nu)^{1/2}$, as shown in Fig 5(b), and found to be 3.45 eV, which is 0.1 eV less than $E_g(\text{dir})$ [24].

Photoactivity Degradation

The photoactivity of the ZnO/NiO nanostructure films is shown in Figure 6. The efficiencies of the

films prepared by CBD and M-CBD by light exposure for 150 min were found to be 76 % relative to 92%, respectively. Accordingly, the efficiency for the decomposition of RB is dependent on the technique.

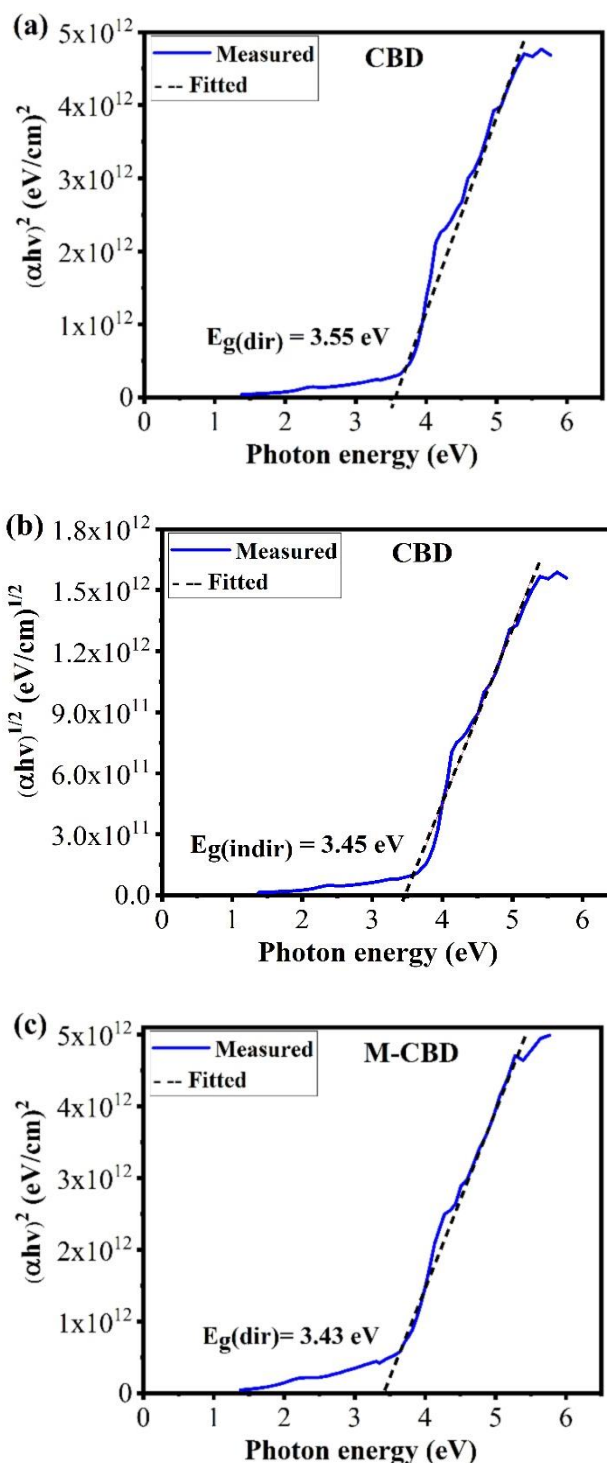


Figure 5. Tauc plots of direct transitions of the ZnO/NiO Nanostructure prepared by (a, b) the CBD and (c) M-CBD techniques.

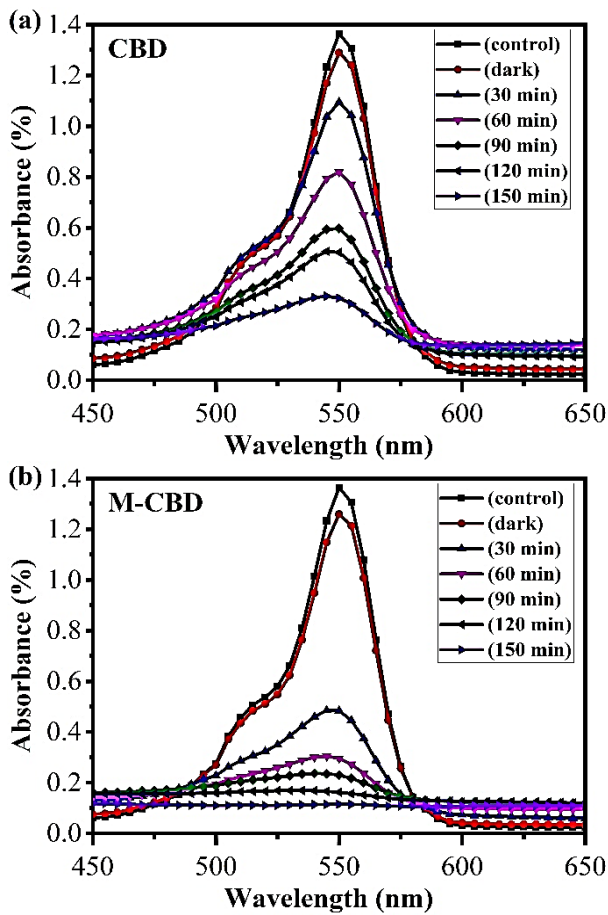


Figure 6. The UV-Vis photodegradation of the RB dye under sunlight by (a) the CBD and (b) the M-CBD routes.

In Figure 7, the change of color due to the degradation of RB by CBD and M-CBD films is demonstrated.

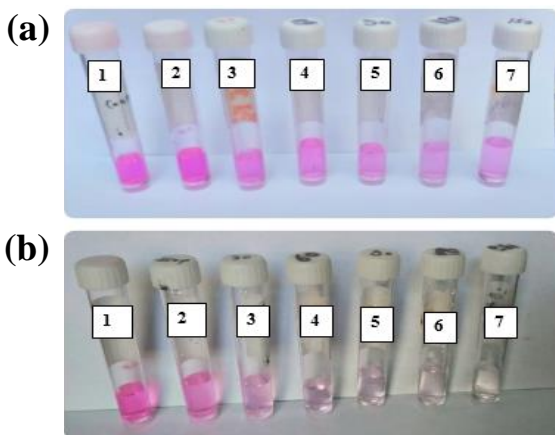


Figure 7. The photodegradation stages of the RB dye with time, (a) CBD, and (b) M-CBD techniques.

The dependence of photoactivity on the exposure time is shown in Figure 8-a at which the decomposition of RB increases with time. Also, as shown in Figure 8-b, the photoactivity of the M-CBD film is highly enhanced relative to the CBD film.

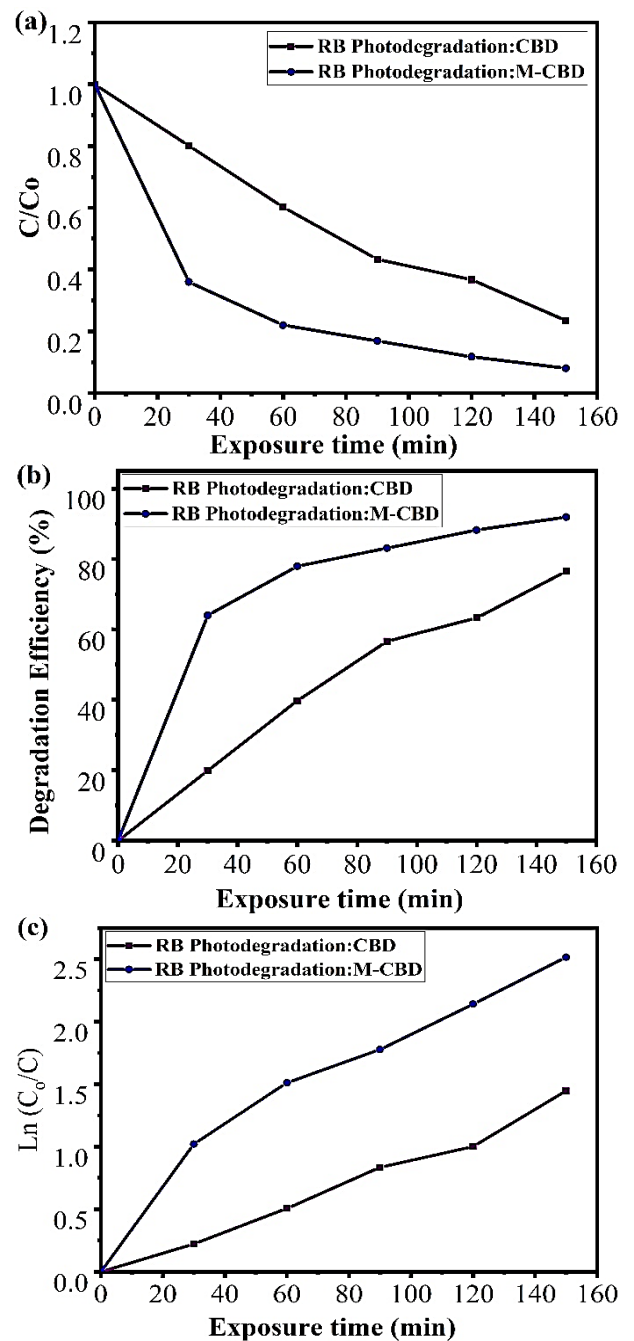


Figure 8. (a) The dependence of the photodegradation of RB on the exposure time, (b) the degradation efficiency of the ZnO/NiO nanostructures, and (c) the first-order kinetics of RB.

The pseudo-first-order rate constant k (min^{-1}) by:

$$\ln(C_0/C) = kt \quad (2)$$

Table 3 demonstrates the values of k (min^{-1}) and photodegradation efficiency of the films.

Table 3. The values of k (min^{-1}) and efficiency for the RB dye photodegradation after 150 min.

Techniques	K (min^{-1})	photodegradation efficiency (%)
CBD	0.00943	76
M-CBD	0.01543	92

CONCLUSIONS

ZnO/NiO heterostructures were prepared using cost-effective CBD and modified CBD techniques. The difference between the photocatalytic of the fabricated heterostructures was investigated. As the results showed that the morphology of ZnO/NiO may change between nanosheets and nanoparticles, the photocatalytic efficacies are different as a result of variation of the structural properties. The decomposition efficacies of the CBD and M-CBD films on RB were 76 % and 92 %, respectively. Accordingly, the mechanism of the technique is inferred to show a crucial role in the results. Hence, the second technique has confirmed the improvement of the photocatalytic activity of the ZnO/NiO heterostructure.

ACKNOWLEDGMENTS

The authors express their thanks to the Department of Physics, College of Science, Mustansiriyah University, Baghdad – Iraq for the supports. (<https://uomustansiriyah.edu.iq/>).

REFERENCES

- [1] W. Xiaa, Y. Wanga, Q. Wangc, and et al, Tubular acceptor-rich ZnO hierarchical heterostructure as an efficient photocatalyst for organic degradation, *Appl. Surf. Sci.*, 506, 145008 (2020).
- [2] T. Alammar and A. V. Mudring, Facile Ultrasound-Assisted Synthesis of ZnO Nanorods in an Ionic Liquid, *Mater. Lett.*, 63, 732–735 (2009).
- [3] L. Li, W. Wang, H. Liu, X. Liu, Q. Song, and S. Ren, First Principles Calculations of Electronic Band Structure and Optical Properties of Cr-Doped ZnO, *J. Phys. Chem. C*, 113 (19), 8460–8464 (2009).
- [4] S. Senobari, A. N.-Ejhih, A comprehensive study on the enhanced photocatalytic activity of CuO-NiO nanoparticles: designing the experiments, *J. Mol. Liq.*, 261, 208–217 (2018).
- [5] C.-J. Chen, C.-H. Liao, K.-C. Hsu, Y.-T. Wu, J.C.S. Wu, P-N junction mechanism on improved NiO/TiO₂ photocatalyst, *Catal. Commun.*, 12, 1307–1310 (2011).
- [6] A. A. Ezhilarasi, J. J. Vijaya, K. Kaviyarasu, and et al., Green synthesis of NiO nanoparticles using *Aegle marmelos* leaf extract for the evaluation of in-vitro cytotoxicity, antibacterial and photocatalytic properties, *J. Photochem. Photobiol. B, Biol.*, 180, 39–50 (2018).
- [7] H. Duan, X. Zheng, S. Yuan, and et al., Sub-3 nm NiO nanoparticles: Controlled synthesis, and photocatalytic activity, *Mater. Lett.*, 81, 245–247 (2012).
- [8] D. Zhang and F. Zeng, Visible light-activated cadmium-doped ZnO nanostructured photocatalyst for the treatment of methylene blue dye, *J. Mater. Sci.*, 47, 2155–2161 (2012).
- [9] A. P. Bhirud, S. D. Sathaye, R. P. Waichal, and et al., An eco-friendly, highly stable and efficient nanostructured p-type N-doped ZnO photocatalyst for environmentally benign solar hydrogen production, *Green Chem.*, 14, 2790–2798 (2012).
- [10] R. Georgekutty, M. K. Seery and S. C. Pillai, A highly efficient Ag-ZnO photocatalyst: synthesis, properties, and mechanism, *J. Phys. Chem. C*, 112, 13563–13570 (2008).
- [11] C. Luo, D. Li, X. Jiang, Y. Zhang, and et al., Preparation of porous micro-nano-structure NiO/ZnO heterojunction and its photocatalytic property, *RSC Adv.*, 4, 3090–3095 (2014).
- [12] R. Saravanan, S. Karthikeyan, V. K. Gupta, and et al., Enhanced photocatalytic activity of ZnO/CuO nanocomposite for the degradation of textile dye on visible light illumination, *Mater. Sci. Eng., C*, 33, 91–98 (2013).
- [13] M. Pirhashemi, A. H.-Yangjeh, S. Rahim, Pouran, Review on the criteria anticipated for the fabrication of highly efficient ZnO-based visible-light-driven photocatalysts, *J. Ind. Eng. Chem.*, 62, 1–25 (2018).
- [14] Z. Zhang, C. Shao, X. Li, and et al., Electrospun nanofibers of p-type NiO/n-type ZnO heterojunctions with enhanced photocatalytic activity, *ACS Appl. Mater. Interfaces*, 2 (10), 2915–2923 (2010).
- [15] M. H. Farzana, S. Meenakshi, Visible light-driven photoactivity of zinc oxide impregnated chitosan beads for the detoxification of textile dyes, *Applied Catalysis A: General*, 503, 124–134 (2015).
- [16] M. Pirhashemi, A. H.-Yangjeh, Facile fabrication of novel ZnO/CoMoO₄ nanocomposites: Highly efficient visible-light-responsive photocatalysts in degradations of different contaminants, *J. Photochem. Photobiol. A*, 363, 31–43 (2018).
- [17] A. Boughelout, R. Macaluso, M. Kechouane, and et al., Photocatalysis of rhodamine B and methyl orange degradation under solar light on ZnO and Cu₂O thin films, *React. Kinet. Mech. Catal.*, 129, 1115–1130 (2020).
- [18] D. A. Lavate, V. J. Sawant, A. S. Khomane, Synthesis, characterization, and catalytic properties of zinc oxide nanoparticles for the treatment of wastewater in the presence of natural sunlight, *Chem. pap.*, 74, 879–885 (2020).
- [19] Z. Lin Wang, Zinc oxide nanostructures: growth, properties, and Applications, *J. Phys.: Condens. Matter*, 16, R829–R858 (2004).
- [20] I. Abdul Rahman, M. T. M. Ayob, and S. Radiman, Enhanced Photocatalytic Performance of NiO-Decorated ZnO Nanowhiskers for Methylene Blue Degradation, *Journal of Nanotechnology*, ID 212694 (2014).

- [21] D. Ao, Z. Li, Y. Fu, and et al., Heterostructured NiO/ZnO nanorod arrays with significantly enhanced H₂S sensing performance, *Nanomaterials* 9 (900) 2019.
- [22] F. Hone and F. Ampong, Effect of deposition temperature on the structural, morphological and optical band gap of lead selenide thin films synthesized by chemical bath deposition method, *Mater. Chem. Phys.*, 183, 320 – 325 (2016).
- [23] D. Nunes, A. Pimentel, A. Gonçalves, and et al., Metal oxide nanostructures for sensor applications, *Semicond. Sci. Technol.* 34, 043001 (2019).
- [24] P. Bhatia and M. Nath, Green synthesis of p-NiO/n-ZnO nanocomposites: Excellent adsorbent for removal of congo red and efficient catalyst for reduction of 4-nitrophenol present in wastewater, *J. Water Process. Eng.*, 33, 101017 (2020).